Proceedings of Meetings on Acoustics

Volume 19, 2013 http://acousticalsociety.org/

ICA 2013 Montreal
Montreal, Canada
2 - 7 June 2013

Engineering Acoustics
Session 2aEA: Directional and Non-Directional Microelectromechanical Microphones

2aEA2. Biomimetic flow sensors for environmental awareness

Gijs J. Krijnen* and Ahmad Dagamseh

***Corresponding author's address: MESA+ Research Institute, University of Twente, p.o. box 217, Enschede, 7500AE, Overijssel, Netherlands, gijs.krijnen@utwente.nl**

Crickets possess hairy organs attached to their abdomen, the so-called cerci. These cerci contain highly flow-sensitive mechanosensors that enable the crickets to monitor the flow-field around them and react to specific stimuli form the environment, e.g. air-movements generated by hunting spiders. Salient is the sensitivity of these sensors, which work at thermal noise threshold levels, and the large number of hairs which, together with the necessary neural processing, allows the cricket to use the cerci as a kind of "flow-camera". Biologists and engineers have been working together in the recent past to regenerate part of the outstanding sensing capabilities of crickets in manmade, bio-inspired flow-sensor arrays. Using micro-electromechanical systems (MEMS) technology sensors are created that are sensitive and show a high degree of directivity. By analyzing the governing physics the sensors have been optimized to the point that currently the electronic interfacing is the limiting factor. Arrays of sensors, interfaced using Frequency Division Multiplexing (FDM), have been demonstrated to enable the tracking of the movement of small spheres.

Published by the Acoustical Society of America through the American Institute of Physics

 [DOI: 10.1121/1.4798960]
Received 23 Jan 2013; published 2 Jun 2013
Proceedings of Meetings on Acoustics, Vol. 19, 030032 (2013)

INTRODUCTION

Many arthropods are equipped with a variety of mechano-sensors that, depending on mechanical transduction principles can provide them with such diverse modalities as angular rate sensing (using the Coriolis effect of wing-beat synchronised so-called halteres) [1, 2], IR sensing capabilities as found in fire-beetles and mediated by IR-absorption and subsequent thermal expansion [3], acceleration sensing, strain-sensing using strain-enhancement in so-called campaniform sensors [4, 5], and flow-sensing by drag-torque induced hair-rotations [6]. In this paper we restrict our-selves to the latter.

An example of animals making extensive use of hair-sensors for environmental awareness are crickets. They possess many hair-sensors over their body, but especially on two pairs of so called cerci they have hundreds of hair-sensors. These hair-sensors provide them with exquisite sensitivity, down to the thermal threshold of about 30 μm/s [7, 8]. At the same time these hairs have a preferable movement in a certain plane due to the elliptical shape of the socket in which the hairs are lodged [9]. In combination with the two cerci and the large number of hairs this provides crickets with highly evolved directivity and an organ that allows them to sense intricate details of even minor flow-patterns. This ability helps them to be successful in, for example, co-evolved predator prey couples, e.g. as found for wood-crickets and wolf-spiders [10].

PHYSICS OF FLOW-SENSING BY HAIRS

The physics of flow-sensing by hair-sensors has been unravelled independently by Humphrey [11] et al. and Shimozawa et al. [12] with initial contributions by Tautz [6, 13] and Gnatzy [14]. The analysis starts with the abstraction of a hair-sensor being an inverted pendulum with moment of inertia J [kgm^2], rotational stiffness S [Nm/rad] and rotational damping R [Nms/rad], vorming a second order mechanical system with the rotational angle ϕ as the single degree of freedom:

$$J\frac{d^2\theta(t)}{dt^2} + R\frac{d\theta(t)}{dt} + S_0\theta(t) = T_0(t) \tag{1}$$

where $T_0(t)$ is the driving drag torque. In general the rotation of the hair will lack behind the flow. The drag-torque needs to be calculated using the difference in air-flow and hair velocity, which is dependent on the distance to the substrate z. In practice the velocity (difference) is rather small allowing to use the Stokes [15] expressions in order to calculate the drag-force. This results in:

$$J\frac{d^2\theta(t)}{dt^2} + R\frac{d\theta(t)}{dt} + S_0\theta(t) = 4\pi\mu G\int_0^L \left[v(t) - z\frac{d\theta}{dt}\right] z dz + \left(\frac{\pi\rho d^2}{4} - \frac{\pi^2\mu G}{g\omega}\right)\int_0^L \left[\frac{dv(t)}{dt} - z\frac{d^2\theta}{dt^2}\right] z dz \tag{2}$$

where $v(t)$ is in the direction $\parallel$ with the substrate ($\perp$ to the hair). Since the terms on the right hand side with time derivatives of θ do not depend on $v(t)$ they can be transfered to the left hand side where they are responsible for additional terms to the moment of inertia (J_ρ, J_μ) and rotational damping (R_μ) [11].

$$\left(J + J_\rho + J_\mu\right)\frac{d^2\theta(t)}{dt^2} + \left(R + R_\mu\right)\frac{d\theta(t)}{dt} + S_0\theta(t) = 4\pi\mu G\int_0^L v(t) z dz + \left(\frac{\pi\rho d^2}{4} - \frac{\pi^2\mu G}{g\omega}\right)\int_0^L \frac{dv(t)}{dt} z dz \tag{3}$$

Note that (J_ρ, J_μ) and (R_μ) need to be calculated only once for a given hair geometry using the integrals implied in eq. 2. For cricket hairs the values of these additive terms can be significant and should not be neglected [11]. For MEMS based bio-inspired hair-sensors these contributions are relatively small for operation in air. However, for sensors working in water, both for bio-inspired as well as natural sensors, these terms may be of comparable value as J and R.

Once the flow velocity $v(t)$ is known the driving torque $T_0(t)$ can be calculated. However, only relative simple flows allow for straightforward modelling. I.e. the boundary layer effects of transient flows are

intricate and need to be determined by numerical schemes like Finite Element Modelling (FEM). Harmonic flows parallel to the substrate may be modelled using the analytic expression [16]:

$$v(t) = V_0 \sin(\omega t) - V_0 e^{-\beta z} \sin(\omega t - \beta z) \tag{4}$$

Substituting 4 in 3 provides all the information needed to calculate the response of the hair-sensors to steady state harmonic driving.

Bio-Insipired Sensors

The bio-inspired sensors are based on a hair-like structure, mounted on a membrane that is suspended by two torsion-beams [17]. When the hair is exposed to flow the drag-forces acting on the hair will provide a drag-torque which will cause the rotation of the hair and the membrane it is sitting on. Electrodes on the membrane form a capacitor with an underlying counter-electrode, either the sensor substrate or the device layer of an SOI wafer. On membrane rotation the capacitances on either side of the torsion-beam will incur capacitance changes, but with opposite sign. Hence, the pair of capacitors can be used to differentially measure the rotation-angle, directly reflecting the flow velocity.

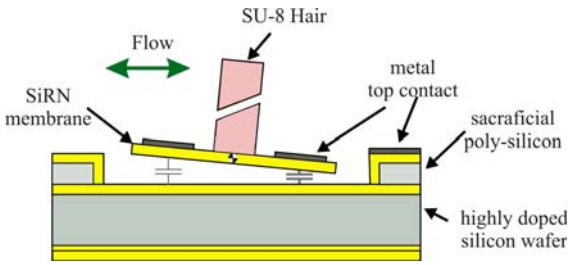

Figure 1: Schematic of the flow-sensitive hair-sensor.

Microfabrication

The fabrication of the hair-sensor (Fig 2, left [18]) starts by etching isolation trenches into the SOI 25 μm thick device layer down to the isolating SiO_2 layer by anisotropic reactive-ion etching (RIE) to form the bottom electrodes (Fig 2-I). A Si_3N_4 layer is deposited over the device layer by low-pressure chemical vapor deposition (LPCVD) (Fig 2-II), for protection during later sacrificial layer etching.

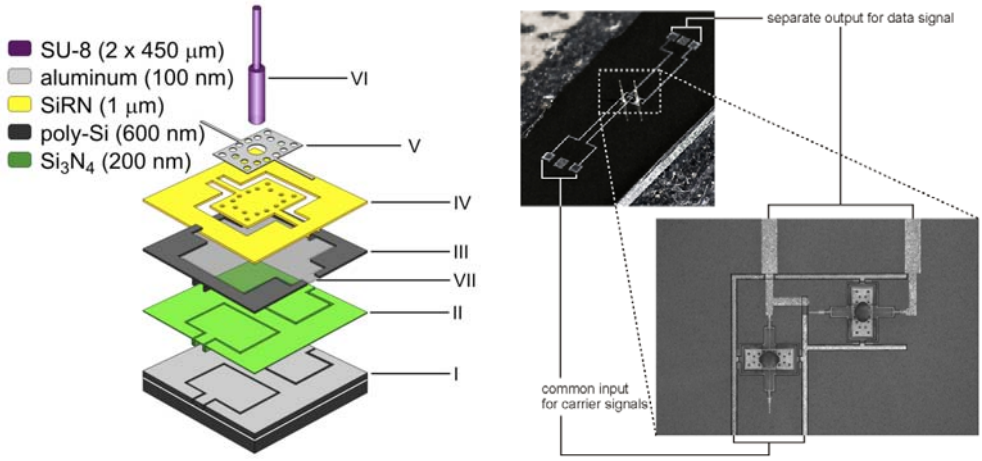

Figure 2: Left: Extruded view of a SOI-based hair-sensor [18]. Right: SEM micrographs of single sensor designs [19].

A sacrificial poly-silicon layer is deposited to a thickness of 600 nm by LPCVD and patterned by reactive-ion etching (RIE) to form protection trenches (Fig 2-III). A second, 1 μm-thick, SiRN layer is deposited by LPCVD and patterned by RIE to form the actual membrane and torsion beams (Fig 2-IV) and to complete the protection of specific areas in the poly-Si layer. The deposition and design of the electrode systems is of prime importance for the sensor performance (due to membrane curvature by possible internal stress in the metal layer). After performing several test runs for stress and resistance measurements of the electrode systems, the thickness of the aluminium layer is set to 100 nm resulting in low- stress, low resistance, electrode systems. After sputtering the aluminium by low-power sputtering at room temperature, the electrode systems are patterned by wet-etching in standard resist developer (Fig 2-V). Use of the developer has several advantages over conventional aluminium etchants, (low etch rate, room temperature etching) and results in the definition of the electrode systems with high fidelity (< 1% deviation with lateral dimensions of the resist mask). For the fabrication of 900 μm-long SU-8 hairs, processing was done by a sequential exposure procedure of two 450 μm-thick SU-8 layers imposed by the maximum exposure thickness of only 700 μm due to UV light adsorption

Fig. 3 shows some of the characteristics of the current generation of sensors as measured on a single sensor. The measurements reflect that our models capture the details of the actual sensors quite well (Fig. 3, left). Fig. 3, middle, shows that our current single hair-sensors are sensitive enough to detect harmonic flows with an amplitude of about 1.06 mm/s at 250 Hz. At the same time the directivity is near to text-book as shown in Fig. 3, right.

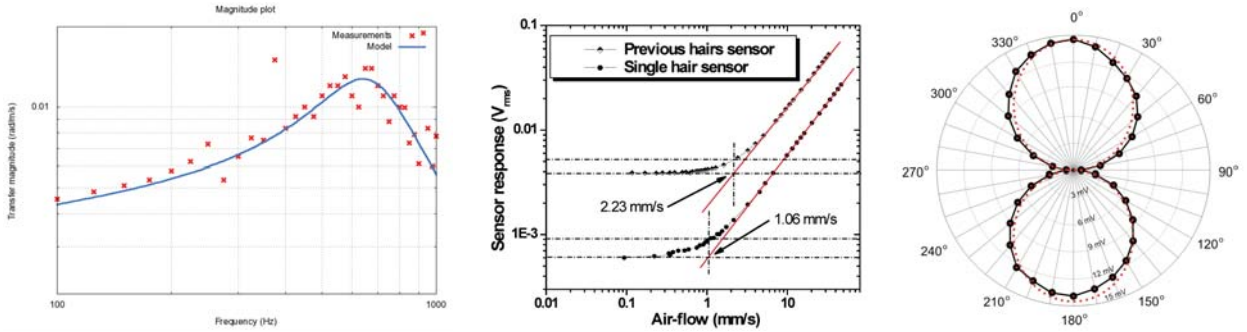

FIGURE 3: Frequency response of a MEMS-based hair-sensor (left), its single-hair threshold at 250 Hz (middle) and directivity (right). (Unpublished data and [20]).

DIRECTIVITY

The sensors have a rotational axis and rotation angle θ in the intended direction with torsional stiffness k_θ. In the direction perpendicular to the 'soft' direction the angle is denoted ϕ and the rotational stiffness is k_ϕ. Under a few assumptions we can try to make a model for the prediction of the directivity:

- The plates are much wider and longer than the gap, allowing the use of the expressions for parallel plate capacitors.
- The flow $\vec{u}(\omega)$ is assumed to have no component perpendicular to the substrate (z-direction). Also pressure difference effects on the plates are neglected and therefore the centre of mass of the plates is assumed not to move in vertical direction.
- The total 2-dimensional rotation of the plates is assumed to be a superposition of the rotations in both (ϕ,θ) directions.

The following two graphs show the difference between right and left capacitances (ΔC) as a function of θ and ϕ and the ratio of the responsivities for rotation in the θ and ϕ directions using the following approximation for the capacitance of the membrane-sides:

$$C_{right} = \epsilon_0 \int_a^L \int_{-w/2}^{w/2} \frac{1}{g_0 + x\theta + y\phi} dxdy \qquad C_{left} = \epsilon_0 \int_a^L \int_{-w/2}^{w/2} \frac{1}{g_0 - x\theta + y\phi} dxdy \tag{5}$$

where g_0 is the effective gap including the nitride contributions. The angular sensitivities are given by:

$$S_\phi = \frac{\partial \Delta C}{\partial \phi} = \epsilon_0 \int_a^L \int_{-w/2}^{w/2} \left[\frac{-y}{(g_0 + x\theta + y\phi)^2} + \frac{y}{(g_0 - x\theta + y\phi)^2} \right] dxdy \tag{6}$$

$$S_\theta = \frac{\partial \Delta C}{\partial \theta} = \epsilon_0 \int_a^L \int_{-w/2}^{w/2} \left[\frac{-x}{(g_0 + x\theta + y\phi)^2} + \frac{-x}{(g_0 - x\theta + y\phi)^2} \right] dxdy \tag{7}$$

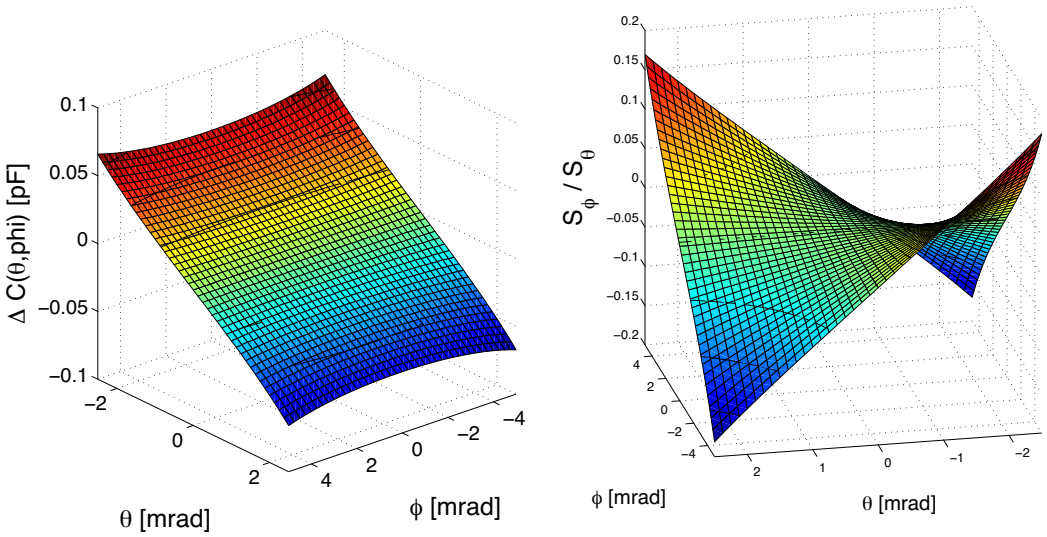

FIGURE 4: Left: differential capacitance as function of θ and ϕ. Right: relative sensitivity (S_ϕ/S_θ) as function of θ and ϕ.

The two graphs in Fig. 4 show that, despite the differential capacitive measurement, it is still possible to pick up flow signals in the ϕ-direction due to the fact that there is a finite change in ΔC with ϕ which originates from the 1 over gap dependence of the capacitance. From Fig. 4, right, it can be deduced that maximum sensitivity in the ϕ direction can be as high as 15% of the sensitivity in the θ direction. However, for this to occur the sensor need already to be in a strong asymmetric situation. On the other hand, for the small rotations normally incurred the cross-talk effects are rather small. Other effects that may reduce the directivity are flow-disturbances due to objects in the vicinity of the sensor (i.e. the wires or components around the sensor). Additional effects will arise in dense sensor structures where angle-dependent viscous coupling between sensors will change the sensitivity dissimilarly in both directions [21–23].

Arrays

The SOI based technology not only serves to reduce parasitics but also allows for crossing electrodes since both the silicon device-layer of the SOI wafer as well as the top aluminium layer, mutually separated by silicon-nitride, allow for electrical connections. The technology enables frequency division multiplexed (FDM, [27]) interfacing to individual sensors in a rectangular array, reducing the number of required electrode connections from $3(n \times m)$ to $2n + m$ for an $n \times m$ array of hair-sensors. Further, this scheme retains the SNR of the hair-sensors at the level they would have had when each single hair-sensor had been individually connected. See Fig. 5, left.

The FDM technique allows for real-time read-out of multiple sensors in parallel. Therefore it enables the observation of spatio-temporal flow-patterns in which the details carry information of the source of the field,

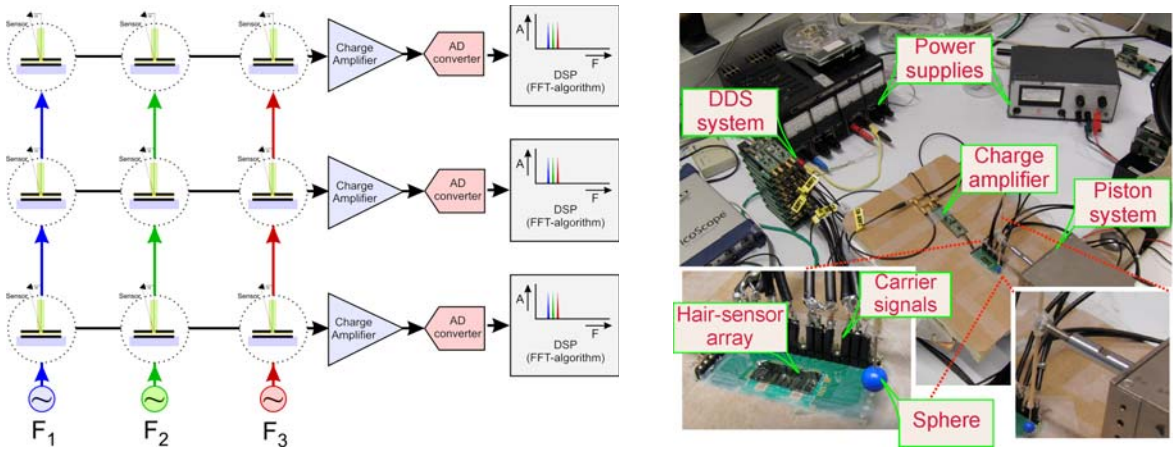

FIGURE 5: Left: FDM reduces the number of connections while retaining the sensor's SNR [19]. Right: setup for transient measurements.

i.e. this type of flow-sensor array in principle allows for the observation (of movement) of objects in the near-field environment, thus acting as a flow-camera. Fig. 7 left, shows an array of sensors, each individually interfaced by FDM.

Transient airflow measurements using artificial hair sensors

For many insects airflow patterns, as observed by means of their hair-sensors, carry valuable information exposing the sources of these flows. There are numerous examples representing transient airflow stimuli such as spider motion [24] and (passing) humming flies [25]. Successful extraction of the characteristics of the spatio-temporal airflow patterns will give us insight in their features and information contained in them.

In most investigations on our artificial hair-sensors the measurements were conducted using sinusoidal airflows [26]. Obviously, using transient signals spatio-temporal information becomes richer and array-measurements will allow to capture important flow events. We measured responses of our biomimetic hair sensors to airflow transients using a sphere with 3 mm radius attached to a piston system to represent the motion of a spider at a distance (D) from the substrate. The sphere moves parallel to the x-axis. A single-chip array consisting of individually addressed (by FDM interfacing) hair sensors is used for flow-detection. Fig. 6, left, shows a photograph of the setup.

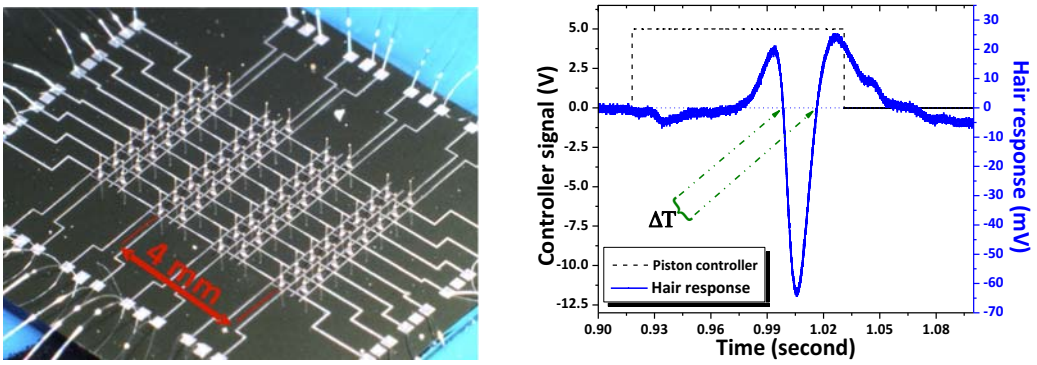

FIGURE 6: Left: microphotograph of an 8×8 array of individually FDM addressable hair-sensors, ordered in pairs with orthogonal directivity [19]. Right: an example of measured hair sensor response (solid) when exposed to a transient flow.

The results show that our hair sensor is able to capture the essential features of the transient airflow field generated by the moving sphere. Interestingly, the hair-sensor response shows strong similarities with a flow-profile generated by a dipole source. Fig. 6 right shows an example of a measured hair-sensor response

due to the sphere movement. The distance to the sphere is encoded in the characteristic points of the flow-field [26]. Hence, it can be derived from the sensor output. In the transient response the time difference between the characteristic points can be translated into position using the piston speed, and subsequently into an estimated distance (D_{est}) between sphere and hair sensor. Fig. 7, left, shows D_{est} versus D using the transient hair response.

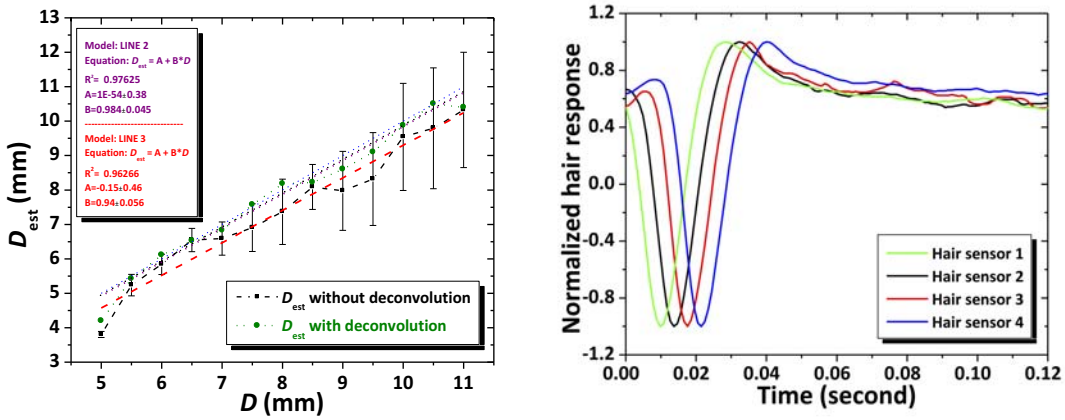

FIGURE 7: Left: D_{est} versus D using transient measurements, before (solid-squares) and after (solid-circles) deconvolving the sensor response. The best linear-line fit for both measurements are compared with ideal linear-line (dotted). D represents the height of the sphere centre relative to the substrate. The error bars represent the uncertainty in determining the zero-crossing points of the measured dipole profile. Right: normalized output of 4 simultaneously measured sensors when exposed to a sphere passing by at certain distance.

Arrays of hair sensors offer us spatial information, specifically if they are measured simultaneously. Here we used FDM [27] to simultaneously measure the transient response of multiple hairs i.e. spatio-temporal airflow pattern measurements. Fig. 7 left shows an image of a single-chip hair-sensor and Fig. 7, right, shows the response of four single-hair sensors in one row, when they are exposed to a transient airflow produced by a moving sphere.

As a first trial, we have been able to detect delays using the signals from four hairs in one row, Fig. 7, right, with sphere propagation speed of 38 cm/s positioned at D = 5 mm with 2 mm separation distance in between each pair of hairs, while using FDM. The measurements show about 4 ms time delay between each two subsequent hair-sensors responses. Fig. 7 right demonstrates the possibility to perform spatio-temporal flow pattern measurements using a single-chip hair sensor array with FDM and to, subsequently, use the features of these flow profiles to determine source parameters.

Measurements like these, in principle, allow to extract the following information. a) The projection of the velocity of the passing sphere in the direction parallel to the row of the sensor array can be determined using the distance between the sensors and the time of flight. b) Once the velocity is known, the distance of the sphere trajectory perpendicular to the row of sensors can be determined from the characteristic points of the dipole-induced signal [28]. c) With the distance to the sphere and its velocity known, the amplitude of the signal can be used to determine the size of the sphere. d) Additional sensors allow to track the motion of the sphere in other directions as well. Clearly, any of the above does not reflect the way crickets use their hair-sensor arrays but it is instructive to see which information a multitude of sensors in principle can uncover.

CONCLUSION

In conclusion, the feasibility of artificial hair-sensor arrays to measure spatio-temporal flow patterns has been demonstrated, opening the possibility to develop high-resolution flow cameras. As an example, we mimicked the cricket-spider escape mechanism using a moving sphere to generate spatio-temporal airflow patterns i.e. transient airflows. The response of single hair-sensors within an array was measured simultaneously using FDM interfacing. Performing source localisation using the measured signals

demonstrates how far we can go with our hair-sensors, either as single sensor or in arrays to detect spatio-temporal airflow fields. The above results may shed some light on the mechanisms that are at work in crickets' flow sensing and how they might exploit spatio-temporal airflow patterns to estimate the occurrence and direction of moving objects in their close environment (both of which have been described in literature [24]).

ACKNOWLEDGMENTS

Many people have contributed to this work over the years. We like to thank in particular Jerome Casas, Thomas Steinmann and other colleagues with whom we collaborated in the EU-projects *Cilia* and *Cicada*, Harmen Droogendijk, Remco Wiegerink, Theo Lammerink, Marcel Dijkstra, Arjan Floris, Remco Sanders, Marcel Kolster, Christiaan Bruinink, Erwin Berenschot, Meint de Boer, Nima Izadi, Ram, Bjorn Hagedoorn, Bas Verlaat, John van Baar, and all the others that we may have forgotten. The research would have been impossible without the grants from the Dutch Technology Foundation (*BioEARS* project) and the European Union.

REFERENCES

[1] G. Nalbach, "The halteres of the blowfly Calliphora", Journal of Comparative Physiology A **175**, 695–708 (1994).

[2] J. Pringle, "The Gyroscopic mechanism of the halteres of diptera", Philosophical Transactions of the Royal Society B: Biological Sciences **233**, 347–384 (1948).

[3] H. Schmitz, H. Soltner, and H. Bousack, "Biomimetic infrared sensors based on photomechanic infrared receptors in pyrophilous ("fire-loving") insects", Sensors Journal, IEEE **12**, 281–288 (2012).

[4] D. H. B. Wicaksono, J. F. V. Vincent, G. Pandraud, G. Craciun, and P. J. French, "Biomimetic strain-sensing microstructure for improved strain sensor: fabrication results and optical characterization", Journal of Micromechanics and Microengineering **15**, S72–S81 (2005).

[5] A. Skordos, P. H. Chan, J. F. V. Vincent, and G. Jeronimidis, "A novel strain sensor based on the campaniform sensillum of insects.", Philosophical transactions. Series A, Mathematical, physical, and engineering sciences **360**, 239–53 (2002).

[6] J. Tautz and H. Markl, "Caterpillars detect flying wasps by hairs sensitive to airborne vibration", Behavioral Ecology and Sociobiology **4**, 101–110 (1978).

[7] T. Shimozawa, J. Murakami, and T. Kumagai, "Cricket wind receptor is sensitive to mechanical energy on the order of kT and utilizes the thermal noise for enhancement of weak signal detection", in *recent developments in auditory mechanics*, 520–526 (2000).

[8] T. Shimozawa, J. Murakami, and T. Kumagai, "Cricket wind receptors: Thermal noise for the highest sensitivity known", Sensors and Sensing in Biology and Engineering 145–157 (2003).

[9] J. P. Miller, S. Krueger, J. J. Heys, and T. Gedeon, "Quantitative characterization of the filiform mechanosensory hair array on the cricket cercus.", PloS one **6**, e27873 (2011).

[10] C. Magal, O. Dangles, P. Caparroy, and J. Casas, "Hair canopy of cricket sensory system tuned to predator signals.", Journal of theoretical biology **241**, 459–66 (2006).

[11] J. A. C. Humphrey and F. G. Barth, "Medium Flow-Sensing Hairs: Biomechanics and Models", Advances in Insect Physiology: Insect Mechanics and Control **34**, 1–80 (2008).

[12] T. Kumagai, T. Shimozawa, and Y. Baba, "Structural scaling and functional design of the cercal wind-receptor hairs of cricket", Journal of Comparative Physiology - A Sensory, Neural, and Behavioral Physiology **183**, 171–186 (1998).

[13] J. Tautz, “Reception of particle oscillation in a medium - an unorthodox sensory capacity”, Naturwissenschaften **66**, 452–461 (1979).

[14] W. Gnatzy and J. Tautz, “Ultrastructure and mechanical properties of an insect mechanoreceptor: stimulus-transmitting structures and sensory apparatus of the cercal filiform hairs of Cryllus”, Cell and Tissue Research **213**, 441–463 (1980).

[15] G. G. Stokes, “On the effect of the internal friction of fluids on the motion of pendulums”, Trans. Cambridge Philos. Soc. **3**, 1–122 (1851).

[16] M. Dijkstra, J. J. V. Baar, R. J. Wiegerink, T. S. J. Lammerink, J. H. D. Boer, and G. J. M. Krijnen, “Artificial sensory hairs based on the flow sensitive receptor hairs of crickets”, Journal of Micromechanics and Microengineering **15**, S132–S138 (2005).

[17] G. J. M. Krijnen, M. Dijkstra, J. J. van Baar, S. S. Shankar, W. J. Kuipers, R. J. H. de Boer, D. Altpeter, T. S. J. Lammerink, and R. Wiegerink, “MEMS based hair flow-sensors as model systems for acoustic perception studies.”, Nanotechnology **17**, S84–9 (2006).

[18] C. M. Bruinink, R. K. Jaganatharaja, M. J. de Boer, E. Berenschot, M. L. Kolster, T. S. J. Lammerink, R. J. Wiegerink, G. J. M. Krijnen, and J. W. Berenschot, “Advancements in technology and design of biomimetic flow-sensor arrays”, Proceedings of the IEEE International Conference on Micro Electro Mechanical Systems (MEMS) 152–155 (2009).

[19] A. M. K. Dagamseh, C. M. Bruinink, H. Droogendijk, R. J. Wiegerink, T. S. J. Lammerink, and G. J. M. Krijnen, “Engineering of biomimetic hair-flow sensor arrays dedicated to high-resolution flow field measurements”, 2010 IEEE Sensors 2251–2254 (2010).

[20] A. M. K. Dagamseh, C. M. Bruinink, R. J. Wiegerink, T. S. J. Lammerink, H. Droogendijk, and G. J. M. Krijnen, “Interfacing of differential-capacitive biomimetic hair flow-sensors for optimal sensitivity”, Journal of Micromechanics and Microengineering **23**, 035010 (2013).

[21] R. K. Jaganatharaja, H. Droogendijk, S. Vats, B. Hagedoorn, C. M. Bruinink, and G. Krijnen, “Unraveling the viscosity-mediated coupling effect in biomimetic hair sensor arrays”, 2011 IEEE 24th International Conference on Micro Electro Mechanical Systems 652–655 (2011).

[22] J. J. Casas, T. T. Steinmann, and G. G. Krijnen, “Why do insects have such a high density of flow-sensing hairs? Insights from the hydromechanics of biomimetic MEMS sensors.”, Journal of the Royal Society, Interface / the Royal Society **7**, 1487–95 (2010).

[23] G. C. Lewin and J. Hallam, “A computational fluid dynamics model of viscous coupling of hairs”, Journal of Comparative Physiology A: Neuroethology, Sensory, Neural, and Behavioral Physiology **196**, 385–395 (2010).

[24] O. Dangles, N. Ory, T. Steinmann, J.-P. Christides, and J. Casas, “Spider’s attack versus cricket’s escape: velocity modes determine success”, Animal Behaviour **72**, 603–610 (2006).

[25] F. G. Barth, J. A. C. Humphrey, U. Wastl, and J. Halbritter, “Dynamics of arthropod filiform hairs . III . Flow patterns related to air movement detection in a spider (Cupiennius salei KEYS .)”, Philosophical Transactions: Biological ecineces **347**, 397–412 (1995).

[26] A. Dagamseh, T. Lammerink, M. Kolster, C. Bruinink, R. Wiegerink, and G. Krijnen, “Dipole-source localization using biomimetic flow-sensor arrays positioned as lateral-line system”, Sensors and Actuators, A: Physical **162**, 355–360 (2010).

[27] A. Dagamseh, R. Wiegerink, T. Lammerink, and G. Krijnen, “Towards a high-resolution flow camera using artificial hair sensor arrays for flow pattern observations.”, Bioinspiration & biomimetics **7**, 046009 (2012).

[28] J.-M. Franosch, M. Lingenheil, and J. van Hemmen, “How a Frog Can Learn What Is Where in the Dark”, Physical Review Letters **95**, 078106 (2005).